8th International Conference on Physical and Numerical Simulation of Materials Processing, ICPNS'16
Seattle Marriott Waterfront, Seattle, Washington, USA, October 14-17, 2016

Numerical Simulation of Heat Transfer in Porous Metals for Cooling Applications

Edgar Avalos and Yuyuan Zhao
School of Engineering, University of Liverpool, Liverpool, L69 3GH, UK

ABSTRACT

Porous metals have low densities and novel physical, mechanical, thermal, electrical and acoustic properties. Hence, they have attracted a large amount of interest over the last few decades. One of their applications is for thermal management in the electronics industry, because of their fluid permeability and thermal conductivity. The heat transfer capability is achieved by the interaction between the internal channels within the porous metal and the coolant flowing throw them. This paper studies the fluid flow and heat transfer in open-cell porous metals manufactured by space holder methods by numerical simulation using software ANSYS-Fluent. A 3D geometric model of the porous structure was created based on the face-centred-cubic arrangement of spheres linked by cylinders. This model allows for different combinations of pore parameters including a wide range of porosity (50-80%), pores size (200-1000 μm) and metal particle sizes (10-75 μm). In this study, water was used as the coolant and copper was selected as the metal matrix. The flow rate was varied in the Darcian and Forchheimer's regimes. The permeability, form drag coefficient and heat transfer coefficient were calculated under a range of conditions. The numerical results showed that permeability increased whereas the form drag coefficient decreased with porosity. Both permeability and form drag coefficient increased with pore size. Increasing flow rate and decreasing porosity led to better heat transfer performance.

Keywords: Porous metal, Numerical simulation, Permeability, Drag form coefficient, Heat transfer coefficient

1. INTRODUCTION

Porous metals, or metallic foams, are metals with pores deliberately integrated in their structure (Zhao, 2013). The pores are of crucial importance because they give new properties to the material. For applications requiring good permeability to fluids, the internal network of the cells in the porous metal must be open. The open-cell porous metals are emerging as an effective material for heat transfer management (Zhang *et al*., 2009).

In active cooling applications using the open cell structures, the cooling system is composed of the porous metal medium and the fluid used as a coolant flowing through the material. In the design of heat exchangers with porous metals, two key properties are important: the heat transfer coefficient and the pressure drop across the sample (Xiao & Zhao, 2013), which are strongly affected by the pore structure (Baloyo & Zhao, 2016).

Porous copper manufactured by the space holder methods, such as the lost carbonate sintering (LCS) process (Zhao et al., 2005), is a promising type of material for use as heat exchangers (Thewsey & Zhao, 2008). However, there is very limited amount of data available on the fluid flow and heat transfer behaviour of this type of materials. Measurements of fluid permeability and heat transfer coefficient are difficult and time-consuming.

Numerical simulation has gained popularity as a reliable tool to study heat transfer in porous media. For example, Teruel and Rizwan-Uddin (2009) numerically calculated the interfacial heat transfer coefficient in porous media. Xin *et al*. (2014) numerically investigated the heat and mass transfer behaviours in porous media for multiphase flow. Hwang and Yang (2012) simulated the heat transfer and fluid flow characteristics in a metallic porous block subjected to a confined turbulent slot jet. Numerical simulation has shown to be a very useful and consistent tool.

Different approaches have been considered in tackling the porous media problem. One methodology is considering the porous media as an arrangement of tube banks in 2D (Teruel & Díaz, 2013). Another practice is creating a representative 3D cell structure (Xu & Jiang, 2008). A different

technique is creating a random walled structure acting as the porous matrix (de Carvalho *et al*., 2015).

This paper studies the fluid flow and heat transfer in open-cell porous metals by numerical simulation using ANSYS-Fluent. A 3D representative elementary volume (REV) has been created to represent the porous structure of LCS porous copper, allowing for different combinations of porosity, pores size and metal particle size.

2. NUMERICAL SIMULATION

2.1 Representative elementary volume (REV)

The REV used to represent the porous structure of LCS porous copper in this study is a FCC unit cell, as shown in Figure 1. The spherical pores are arranged the same way as that the atoms are arranged in the FCC structure. The pores are connected by cylindrical open channels at the contact points. The porosity of the REV is varied by changing the radius of the cylinder, r_c, and the distance between the centres of the neighbouring spheres, l_s.

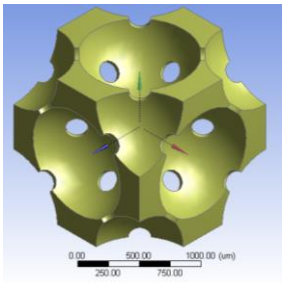

Figure 1 *Representative elementary volume*

The radius of the cylinder is selected to reflect the size of the necks or windows connecting neighbouring pores in the LCS porous copper, which is determined by the sizes of the $\mathrm{K_2CO_3}$ and Cu particles and can be calculated by (Zhao, 2003; Diao *et al*., 2015):

$$A_{sc} = \frac{\pi}{2}\left(d_{K_2CO_3}\right)^2\left(1 - \frac{(\varphi+2)}{\sqrt{\varphi^2+6\varphi+5}}\right) \qquad (1)$$

where A_{sc} is the area of the neck, $d_{K_2CO_3}$ is the K_2CO_3 particle diameter, and φ is the K_2CO_3-to-Cu particle size ratio, i.e., the ratio between the diameters of the K_2CO_3 and Cu particles.

The coordination number, or the number of contacts of a sphere with its neighbours, is 12 in the FCC structure. In LCS porous metals, however, the coordination number, ω, is much lower and can be estimated by:

$$\omega = \frac{2}{\left(1 - \frac{(\varphi+2)}{\sqrt{\varphi^2+6\varphi+5}}\right)\left(1-\varphi+\frac{\varphi}{\varepsilon}\right)} \qquad (2)$$

where ε is the porosity.

To account for this difference, the total area of the necks in the REV is considered to be equal to the total area of the necks of a pore in the real porous material. The radius of the cylinders used in the REV can therefore be obtained by:

$$r_c = \sqrt{\frac{\omega \cdot A_{sc}}{12\pi}} \qquad (3)$$

Given the pore size, $\mathrm{d_{K_2CO_3}}$, the cylinder radius, r_c, and the porosity, ε, the distance between the centres of the neighbouring spheres, l_s, can be determined.

The values of the cylinder radius and the distance between the centres of the neighbouring spheres for each combination of pore size and porosity are presented in Table 1. In this study, the Cu particle size is fixed as $50\ \mu\mathrm{m}$.

Table 1 *Cylinder radius and distance between neighbouring spheres for the REVs*

	Pore diameter (μm)							
	400		**600**		**800**		**1000**	
ε	r_c (μm)	l_s (μm)	r_c (μm)	l_s (μm)	r_c (μm)	l_s (μm)	r_c (μm)	l_s (μm)
50%	37.76	463.87	47.33	691.85	55.34	919.85	62.36	1147.60
60%	45.01	435.44	56.89	649.85	66.81	864.30	75.49	1078.60
65%	49.17	423.11	62.48	631.70	73.59	840.47	83.30	1049.05
70%	53.82	411.61	68.86	614.93	81.41	818.50	92.37	1021.90
75%	59.15	400.70	76.32	599.13	90.67	797.82	103.21	996.50
80%	65.40	390.03	85.33	583.75	102.05	777.93	116.67	972.15

2.2 Boundary conditions

Simulations were carried out using ANSYS Fluent CFD with different REVs to account for different combinations of pore size and porosity as shown in Table 1. The parameters considered for this analysis were pore size, porosity and volumetric flow rate.

The computational domain is composed of three parts: a fluid channel long enough for the fluid to be fully developed, the REV in the fluid channel that represents the porous metal, and a solid copper block underneath the REV supplying a constant heat flux.

A constant heat flux (J = 250 kW/m^2) was set at the bottom of the solid block. The heat is transferred from the block to the REV via conduction and is removed from the REV by forced convection using water. The top of the domain was set as zero heat flux. The other two sides of the domain were set as symmetric. The initial temperature for the whole domain was set as 293 K.

The velocity, pressure, and temperature fields in the fluid phase of the domain were investigated. The governing equations were solved numerically and numerical computations were performed for a wide range of porosity (50% - 80%), pore size ($200 - 1000$ μm), and Darcian flow velocity (0.02 – 0.3 m/s) or flow rate (0.2 – 1.8 l/min).

In this study, the overall quality of the mesh was >0.9 in all cases. The numerical computations were considered to be converged when the residuals of the variables were lowered by six orders of magnitude (i.e. $\leq 10^{-6}$). Double precision conditions were selected at solver to minimize the possibility of errors.

2.1 Permeability and form drag coefficient

According to Darcy's law for unidirectional flow through a porous medium in creeping flow regime, the pressure drop per unit length is proportional to the superficial fluid velocity:

$$\frac{\Delta P}{\Delta l} = \frac{\mu}{K} u \qquad (4)$$

where ΔP is the pressure drop between the inlet and outlet of the porous media, Δl is the length of the porous media, μ is the viscosity of the fluid, u is the Darcian velocity of the fluid (i.e., flow rate divided by the cross sectional area), and K is the permeability of the porous media.

If the Reynolds number, *Re*, increases to a critical value, the fluid will become turbulent and this relationship will change to nonlinear and the Forchheimer equation needs to be used (Despois & Mortensen, 2005):

$$\frac{\Delta P}{\Delta L} = \frac{\mu u}{K} + \rho C u^2 \qquad (5)$$

where ρ is the density of the fluid, and C is the Forchheimer's coefficient, or from drag coefficient.

In this study, Equation (5) was used to determine the permeability, K, and form drag coefficient, C, from the pressure drop values.

2.2 Heat transfer coefficient

The heat flux and heat transfer coefficient in the LCS porous copper is related by Newton's cooling law:

$$J = h(T_b - T_{in}) \qquad (6)$$

where J is the input heat flux, h is the heat transfer coefficient, T_b is the temperature at the contact point between the heat source and the LCS porous copper, and T_{in} is the temperature of the water at the inlet. In this study, Equation (6) was used to determine the heat transfer coefficient, *h*, from the temperature of the heat block.

3. RESULTS AND DISCCUSION

3.1 Permeability and form drag coefficient

The relationship between pressure drop and Darcian velocity for samples with a pore size of 1000 μm and different porosities is shown in Figure 2. It is clear that the trend is not linear and the form drag coefficient needs to be considered to account for the inertial effects.

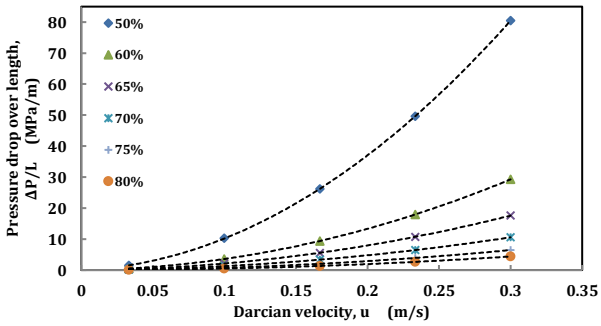

Figure 2 *Relationship between pressure drop and Darcian velocity for samples with a pore diameter of 1000 μm and different porosities*

To obtain permeability, K, and form drag coefficient, *C*, Equation (5) can be rearranged to give a linear relationship between ΔP and u such that:

$$\frac{\Delta P}{L \cdot u} = \frac{\mu}{K} + \rho C u \qquad (7)$$

The values of *K* and *C* were thus obtained by linear regression of the data to Equation (7).

The variations of permeability and form drag coefficient with porosity are shown in Figures 3(a) and (b), respectively. As expected, permeability increased with porosity whereas form drag coefficient decreased with porosity, because less frontal surface area in the solid material generates less drag force against the fluid

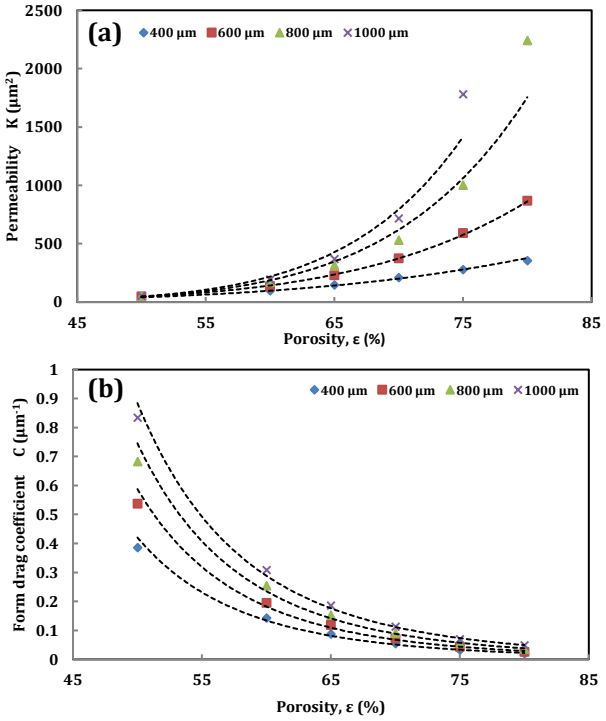

Figure 3 *Relationships between (a) permeability and porosity and (b) form drag coefficient and porosity*

In the literature, the form drag coefficient is sometimes defined in terms of permeability and a drag force coefficient (e.g., Mancin *et al*., 2012):

$$C = \frac{C_f}{\sqrt{K}} \qquad (8)$$

where C_f is the drag force coefficient.

Figure 4 shows the log-log plots between form drag coefficient and permeability. It is clear that the data in the current study do not follow Equation (8), but can be described in the following form:

$$C = C_f K^{-m} \qquad (9)$$

where *m* is a constant for any fixed pore size.

The values for the exponential term and drag force coefficient for different pore sizes, obtained from linear regressions of the data in Figure 4, are presented in Table 2. The value of the exponential term m is not constant, but it approaches to 0.5 when pore size is increased. The drag force coefficient also increases with pore size.

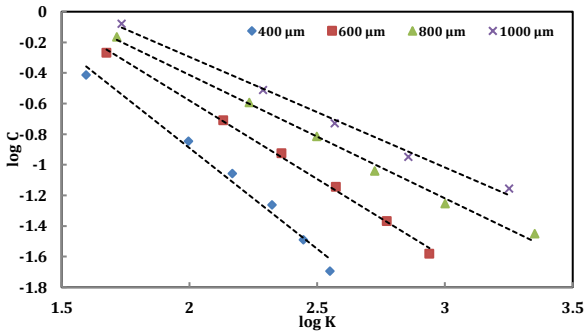

Figure 4 *Relationship between form drag coefficient and permeability*

Table 2 *Exponential term and drag force coefficient*

Pore size (µm)	m	C_f
400	1.3184	3.156299
600	1.0264	3.320117
800	0.8065	4.360558
1000	0.7223	5.734497

3.2 Heat transfer coefficient

The relationships between heat transfer coefficient and water flow rate for the porosities of 50% and 80% are shown in Figure 5(a) and (b), respectively.

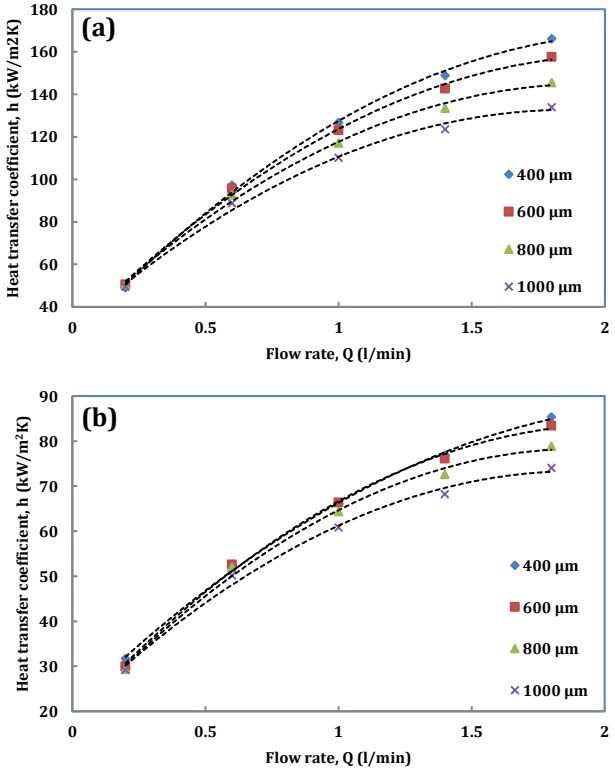

Figure 5 *Heat transfer coefficient of REVs with a porosity of (a) 50% and (b) 80%*

It can be seen that the heat transfer coefficient increased rapidly with flow rate. The effect of pore size can be seen here as well. Although at low flow rates the effect of pore size was negligible, at higher flow rates, h was increased by about 5% to 8% when pore size was decreased.

The relationships between heat transfer coefficient and porosity for pore sizes of $400\ \mu m$ and $1000\ \mu m$ are shown in Figures 6(a) and (b), respectively. A linear relationship exists between the heat transfer coefficient and porosity for all flow rates. At all cases, the best heat transfer coefficient was achieved with higher flow rates. Once again, it can be seen that pore size has little influence on the heat transfer coefficient.

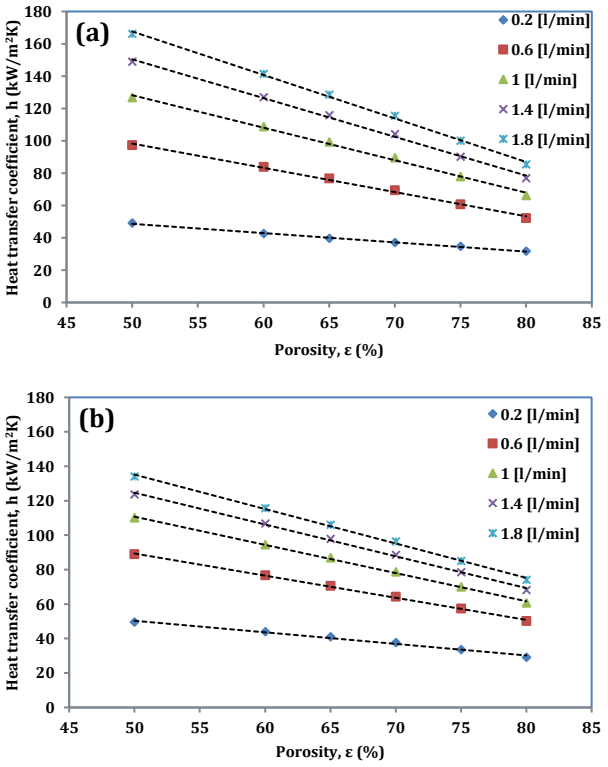

Figure 6 *Heat transfer coefficient of REVs with pore size of (a) 400 µm and (b)1000 µm*

4. CONCLUSIONS

This paper presented a 3D geometric model for numerical simulation of liquid flow and heat transfer in open cell porous media with different combinations of pore parameters including porosity, pore size and fluid flow rate. The numerical results showed that permeability increased whereas the form drag coefficient decreased with porosity; both permeability and form drag coefficient increased with pore size; heat transfer increased with flow rate but decreased with porosity. Pore size had very little effect on heat transfer coefficient.

ACKNOWLEDGMENTS

This work has been supported by the Engineering and Physical Sciences Research Council (Grant No. EP/N006550/1). Avalos would like to thank CONACYT and SEP for a PhD scholarship. Data files for the figures in this paper may be accessed at http://datacat.liverpool.ac.uk/id/eprint/150.

REFERENCES

Baloyo, J. M., & Zhao, Y. (2015). Heat transfer performance of micro-porous copper foams with homogeneous and hybrid structures manufactured by lost carbonate sintering. MRS Proceedings, *1779*, mrss15-2095240.

de Carvalho, T. P., Morvan, H., Hargreaves, D., Oun, H., & Kennedy, A. (2015). Experimental and tomography-based CFD investigations of the flow in open cell metal foams with application ot aero engine separators. In *Proceedings of ASME Turbo Expo 2015: Turbine Technical Conference and Exposition GT2015* (pp. 1–11).

Despois, J., & Mortensen, A. (2005). Permeability of open-pore microcellular materials. *Acta Materialia*, *53*(5), 1381–1388.

Diao, K. K., Xiao, Z., & Zhao, Y. (2015). Specific surface areas of porous Cu manufactured by Lost Carbonate Sintering: Measurements by quantitative stereology and cyclic voltammetry. *Materials Chemistry and Physics*, *162*, 571–579.

Hwang, M.-L., & Yang, Y.-T. (2012). Numerical simulation of turbulent fluid flow and heat transfer characteristics in metallic porous block subjected to a confined slot jet. *International Journal of Thermal Sciences*, *55*, 31–39.

Mancin, S., Zilio, C., Diani, A., & Rossetto, L. (2012). Experimental air heat transfer and pressure drop through copper foams. *Experimental Thermal and Fluid Science*, *36*, 224–232.

Teruel, F. E., & Díaz, L. (2013). Calculation of the interfacial heat transfer coefficient in porous media employing numerical simulations. *International Journal of Heat and Mass Transfer*, *60*, 406–412.

Teruel, F. E., & Rizwan-uddin. (2009). Characterization of a porous medium employing numerical tools: Permeability and pressure-drop from Darcy to turbulence. *International Journal of Heat and Mass Transfer*, *52*(25-26), 5878–5888.

Thewsey, D. J., & Zhao, Y. (2008). Thermal conductivity of porous copper manufactured by the lost carbonate sintering process. *Physica Status Solidi (a)*, *205*(5), 1126–1131.

Xiao, Z., & Zhao, Y. (2013). Heat transfer coefficient of porous copper with homogeneous and hybrid structures in active cooling. *Journal of Materials Research*, *28*(17), 2545–2553.

Xin, C., Rao, Z., You, X., Song, Z., & Han, D. (2014). Numerical investigation of vapor–liquid heat and mass transfer in porous media. *Energy Conversion and Management*, *78*, 1–7.

Xu, R.-N., & Jiang, P.-X. (2008). Numerical simulation of fluid flow in microporous media. *International Journal of Heat and Fluid Flow*, *29*(5), 1447–1455.

Zhang, L., Mullen, D., Lynn, K., & Zhao, Y. (2009). Heat transfer

performance of porous copper fabricated by the lost carbonate sintering process, *1188*, 213-218.

Zhao, Y. (2003). Stochastic modelling of removability of NaCl in sintering and dissolution process to produce Al foams. *Journal of Porous Materials*, *10*(2), 105–111.

Zhao, Y., Fung, T., Zhang, L. P., & Zhang, F. L. (2005). Lost carbonate sintering process for manufacturing metal foams. *Scripta Materialia*, *52*(4), 295–298.

Zhao, Y. (2013). Porous metallic materials produced by P/M methods. *Journal of Powder Metallurgy & Mining*, *02*(03), 2–3.